



Polarization independent guided-mode resonance in liquid crystal-based polarization gratings

ZHIYONG YANG,^{1,2}  TAO ZHAN,^{1,2}  AND SHIN-TSON WU^{1,*} 

¹CREOL, The College of Optics & Photonics, University of Central Florida, Orlando, Florida 32816, USA

²These authors contributed equally to this work

*swu@creol.ucf.edu

Abstract: Polarization independent guided-mode resonance (GMR) in a one-dimensional liquid crystal-based polarization grating is demonstrated. The proposed GMR filter consists of a liquid crystal layer and two glass substrates. The resonance location and bandwidth are investigated through anisotropic rigorous coupled-wave analysis. This type of polarization independent GMR filters also manifest strong electric field enhancements and ultra-narrow spectral bandwidths, offering great potential for applications with unpolarized light sources.

© 2020 Optical Society of America under the terms of the [OSA Open Access Publishing Agreement](#)

1. Introduction

The guided-mode resonance (GMR) is a unique phenomenon where a diffracted order is phase matched to a leaky mode of the waveguide [1]. Due to multi-beam interference, narrowband resonant peaks can be formed using resonant waveguide gratings [2], making them suitable for optical notch filters [3–5], lasers feedback elements [6], and refractive index biosensors [7]. The electrical field enhancement in GMR filters has also been studied by Wei, et al. [8], which extends their application to fluorescence enhancement [9].

Most GMRs behave differently depending on the polarization states of an incident beam because of the different propagation constants for the TE and TM guided modes. Therefore, it poses limitation to many applications where a nonpolarizing light source is used. Many efforts have been devoted to realizing polarization independence based on two-dimensional (2D) and one-dimensional (1D) gratings for more than two decades. Peng and Morris [10,11] theoretically investigated and experimentally demonstrated the resonant anomalies in 2D gratings and polarization independent narrowband GMRs. Mizutani, et al. [12] proposed a rhombic grating structure whose symmetric plane coincided with the incident plane to realize nonpolarizing GMRs at an oblique incidence. Two orthogonally cross-integrated GMR gratings were reported by Kintaka, et al. [13] to achieve polarization independence. Although a 2D grating can provide more degrees of freedom than its 1D counterpart, its geometrical structure and fabrication process are more complicated. Ding and Magnusson [14] designed a polarization independent reflector based on a 1D single-layer waveguide grating with a large modulation depth, but the spectral bandwidth for the TE and TM polarizations was considerably different. Hu, et al. [15] harnessed possible intersections of dispersion curves for the TE and TM leaky modes in a 1D periodic waveguide to realize polarization independent GMRs at an oblique incidence. The resonant wavelength for the TE and TM polarizations is accordant, however, the spectral bandwidth is still not matched.

In this paper, a novel structure based on 1D liquid crystal (LC) polarization gratings (PGs) is proposed to realize polarization independent GMRs. Sun and Wang [16] reported an electrically tunable polarization independent GMR filter based on polymer-dispersed liquid crystal (PDLC). However, the polarization independence was not fulfilled by the PDLC but by a square 2D aluminum grating. Concerning previous LC-based GMRs, the LCs are employed to achieve an

electrically tunable [16] or switchable [17] functionality, but little attention is paid to exploiting the LC-based Pancharatnam-Berry phase [18] for polarization independent GMRs. Compared to previous polarization independent approaches, our method stands out due to its polarization independent resonance location and bandwidth, and a relatively simple device structure. To study the field distributions and enhancements of GMRs in PGs, we first modify the field solution [19] and formulate the stable field distribution by anisotropic Rigorous Coupled-Wave Analysis (RCWA). Then specific structural parameters to realize polarization independent GMRs are searched and optimized. The effects of the LC birefringence (Δn) on spectral bandwidths and electric field enhancements are investigated via selecting three commercial LC mixtures as calculation examples.

2. RCWA formulation

Wang, et al. [1] thoroughly studied GMR in planar gratings by RCWA [20]. They pointed out that RCWA could give detailed physical explanations to GMR. Besides that, in term of searching and optimizing numerous structural parameters [21], RCWA provides a much faster simulation speed than those purely numerical methods. Rumpf [19] formulated a general field solution, but the electromagnetic fields involved evanescent waves could be numerically unstable.

Starting with an incident plane wave having a single frequency denoted by ω , Maxwell equations that govern the light propagation in the LC PG without free charge and current are given by:

$$\nabla \times \mathbf{E} = -j\omega\mu_0\mathbf{H}, \quad (1)$$

$$\nabla \times \mathbf{H} = j\omega\epsilon_0[\boldsymbol{\epsilon}]\mathbf{E}. \quad (2)$$

For a nematic LC, the anisotropy axis orientation is in the direction of the LC directors, as Fig. 1 depicts. The propagation vector \mathbf{k} lies in the x - z plane, and Λ and d is the grating periodicity and thickness, respectively.

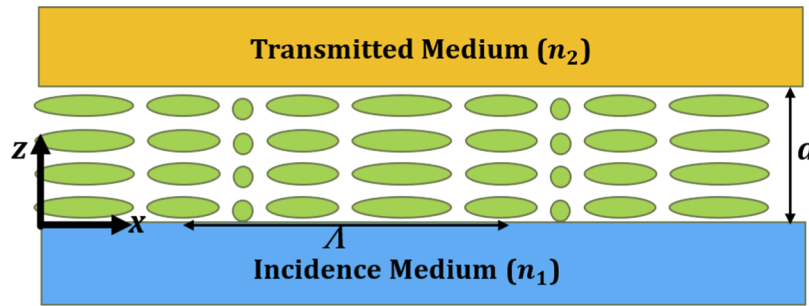


Fig. 1. Device structure of the proposed LC polarization grating.

For a specific direction of the LC directors, the dielectric tensor $[\boldsymbol{\epsilon}]$ is given by [22]:

$$[\boldsymbol{\epsilon}] = \begin{bmatrix} n_o^2 + (n_e^2 - n_o^2)\cos^2\phi & (n_e^2 - n_o^2)\sin\phi\cos\phi & 0 \\ (n_e^2 - n_o^2)\sin\phi\cos\phi & n_o^2 + (n_e^2 - n_o^2)\sin^2\phi & 0 \\ 0 & 0 & n_o^2 \end{bmatrix}, \quad (3)$$

where ϕ is the azimuthal orientation angle between the x axis and the projection of the LC directors on the x - y plane, the pretilt angle of the LC directors is assumed to be zero, and n_o and n_e are the LC ordinary and extraordinary refractive index, respectively. The LC directors periodically vary along the x -axis in Fig. 1, which can be mathematically expressed as $\phi(x)=\pi x/\Lambda$.

Next, the fields in the grating region are represented by a periodic Fourier expansion with spatially variant coefficients, and each periodic permittivity component is expanded in Fourier series. The expanded fields and permittivity components are given by:

$$E_i(x, z) = \sum_{m=-\infty}^{\infty} S_{i,m}(z)e^{-jk_{x,m}x}, \tag{4}$$

$$H_i(x, z) = \sum_{m=-\infty}^{\infty} U_{i,m}(z)e^{-jk_{x,m}x}, \tag{5}$$

$$\epsilon_{ij}(x) = \sum_{h=-1}^1 \epsilon_{ij,h} e^{jh\frac{2\pi}{\Lambda}x}, \tag{6}$$

where $k_{x,m}=k_{x,0}-2\pi m/\Lambda$, $S_{i,m}(z)$ and $U_{i,m}(z)$ are the amplitudes of the m -th field harmonic in the grating region, and subscripts i and j refer to any one of x, y, z . For mathematical simplicity, the magnetic field is normalized according to $\tilde{\mathbf{H}} = -j\sqrt{\mu_0/\epsilon_0}\mathbf{H}$. The tangential wavevector and z coordinate are normalized by $\tilde{k}_{x,m} = k_{x,m}/k_0$ and $\tilde{z} = k_0z$, respectively. Then we insert Eq. (4), Eq. (5) and Eq. (6) into Eq. (1) and Eq. (2), resulting in following six matrix equations:

$$\frac{d}{d\tilde{z}}u_y = -[\epsilon_{xx}]s_x - [\epsilon_{xy}]s_y, \tag{7}$$

$$\frac{d}{d\tilde{z}}u_x + j\tilde{K}_xu_z = [\epsilon_{yx}]s_x + [\epsilon_{yy}]s_y, \tag{8}$$

$$-j\tilde{K}_xu_y = [\epsilon_{zz}]s_z, \tag{9}$$

$$\frac{d}{d\tilde{z}}s_y = -u_x, \tag{10}$$

$$\frac{d}{d\tilde{z}}s_x + j\tilde{K}_xs_z = u_y, \tag{11}$$

$$\tilde{K}_xs_y = ju_z, \tag{12}$$

where $s_i = [S_{i,-M}, \dots, S_{i,M}]^T$, $u_i = [U_{i,-M}, \dots, U_{i,M}]^T$, $[\epsilon_{ij}]$ is the convolution matrix formed by $\epsilon_{ij,mp} = \epsilon_{ij,m-p}$, and \tilde{K}_x is the diagonal matrix constructed by $k_{x,m}$. The infinite series expansion is truncated to a finite number of harmonics. Then two coupled equations between u_x, u_y and s_x, s_y can be obtained via expressing the longitudinal field components u_z, s_z in terms of s_y, u_y :

$$\frac{d}{d\tilde{z}} \begin{bmatrix} u_x \\ u_y \end{bmatrix} = Q \begin{bmatrix} s_x \\ s_y \end{bmatrix} = \begin{bmatrix} [\epsilon_{yx}] & [\epsilon_{yy}] - \tilde{K}_x I^{-1} \tilde{K}_x \\ -[\epsilon_{xx}] & -[\epsilon_{xy}] \end{bmatrix} \begin{bmatrix} s_x \\ s_y \end{bmatrix}, \tag{13}$$

$$\frac{d}{d\tilde{z}} \begin{bmatrix} s_x \\ s_y \end{bmatrix} = P \begin{bmatrix} u_x \\ u_y \end{bmatrix} = \begin{bmatrix} \mathbf{O} & \mathbf{I} - \tilde{K}_x[\epsilon_{zz}]^{-1}\tilde{K}_x \\ -\mathbf{I} & \mathbf{O} \end{bmatrix} \begin{bmatrix} u_x \\ u_y \end{bmatrix}, \tag{14}$$

where \mathbf{I} and \mathbf{O} refer to the unitary and zero matrix respectively. The solutions for the coupled wave equations can be combined as:

$$\begin{bmatrix} s_x \\ s_y \\ u_x \\ u_y \end{bmatrix} = \begin{bmatrix} W & W \\ -V & V \end{bmatrix} \begin{bmatrix} X(z) & \mathbf{O} \\ \mathbf{O} & X(d-z) \end{bmatrix} \begin{bmatrix} c^+ \\ c^- \end{bmatrix}, \tag{15}$$

where c^+ and c^- are column vectors representing the amplitude coefficients of the forward and backward propagations of space harmonics respectively, $X(z)=exp(-\lambda k_0z)$, W and λ^2 are the

eigenvectors and eigenvalues of the matrix $P \times Q$, and $V = QW\lambda^{-1}$. Equation (15) is numerically stable even if evanescent waves are present. Finally, the same procedure is repeated for the superstrate and substrate, then the tangential fields at the two boundaries are matched to give the expression for the scattering matrix:

$$\begin{bmatrix} W_1 & W_1 \\ -V_1 & V_1 \end{bmatrix} \begin{bmatrix} c_1^+ \\ c_1^- \end{bmatrix} = \begin{bmatrix} W & W \\ -V & V \end{bmatrix} \begin{bmatrix} I & O \\ O & X(d) \end{bmatrix} \begin{bmatrix} c^+ \\ c^- \end{bmatrix}, \quad (16)$$

$$\begin{bmatrix} W & W \\ -V & V \end{bmatrix} \begin{bmatrix} X(d) & O \\ O & I \end{bmatrix} \begin{bmatrix} c^+ \\ c^- \end{bmatrix} = \begin{bmatrix} W_2 & W_2 \\ -V_2 & V_2 \end{bmatrix} \begin{bmatrix} c_2^+ \\ c_2^- \end{bmatrix}, \quad (17)$$

$$\begin{bmatrix} c_1^- \\ c_2^+ \end{bmatrix} = \begin{bmatrix} S_{11} & S_{12} \\ S_{21} & S_{22} \end{bmatrix} \begin{bmatrix} c_1^+ \\ c_2^- \end{bmatrix}, \quad (18)$$

where the subscripts 1, 2 signify the incident region I and the transmitted region II, respectively. Without introducing a gap medium, a backward input is not present. Once the three-dimensional (3D) polarization denoted by (p_x, p_y, p_z) of the incident light is given, the transverse components of the reflected and transmitted fields can be obtained by solving Eq. (16), Eq. (17) and Eq. (18). The derived formula for the scattering matrix is the same as that published in [19], although the form of the field solution is different. The longitudinal components in two homogenous regions can be derived from the divergence equation. Thus, the three amplitude components of electric fields in regions I and II have been manifested. Then s_x, s_y, u_x and u_y will be correctly given in Eq. (15) as long as c^+ and c^- are numerically stable. $X(-d)$ may become very large for evanescent waves, thus causing the numerical instability. To eliminate the term $X(-d)$ in the solution for c^+ and c^- , Eq. (16) and Eq. (17) must be jointly solved for c^+ and c^- , which leads to:

$$\begin{cases} 2c^+ = (W^{-1} + V^{-1}V_1)c_1^+ + (W^{-1} - V^{-1}V_1)c_1^- \\ 2c^- = (W^{-1} - V^{-1}V_2)c_2^+ + (W^{-1} + V^{-1}V_2)c_2^- \end{cases}. \quad (19)$$

The remaining s_z can also be calculated by Eq. (9), and the solution is $s_z = -j[\epsilon_{zz}]^{-1}\tilde{K}_x u_y$. Thus, the three amplitude components of electric fields in the grating region have also been derived. Since transverse and longitudinal amplitude coefficients in the three regions have been obtained above, the 3D field distributions are summarized as follows:

$$E_i(x, z) = \sum_{m=-M}^M S_{i,m}(z) e^{-jk_{x,m}x} \quad (0 < z < d), \quad (20)$$

$$E_{I,i}(x, z) = p_i e^{-j(k_{x,0}x + k_{1,z,0}z)} + \sum_{m=-M}^M C_{1,i,m}^- e^{-j(k_{x,m}x - k_{1,z,m}z)} \quad (z < 0), \quad (21)$$

$$E_{II,i}(x, z) = \sum_{m=-M}^M C_{2,i,m}^+ e^{-j(k_{x,m}x + k_{2,z,m}(z-d))} \quad (z > d), \quad (22)$$

where the subscript i refers to any one of x, y, z , and $S_{i,m}, C_{1,i,m}^-$, and $C_{2,i,m}^+$ are the m -th harmonic element of the column vector $s_i, c_{1,i}^-$, and $c_{2,i}^+$, respectively.

3. Polarization-independent GMRs

The proposed waveguide grating structure is simply composed of a LC PG between two identical glass substrates. The proposed structure can function as a GMR filter based on the mode matching: the real part of a mode propagation constant in a period leaky waveguide approaches the tangential propagation constant of a diffracted order, strong resonance can result in a narrowband reflection peak. Incident waves can be coupled into certain waveguide modes due to the transverse momentum additional provided by the grating, however, guided modes are not stable and thus become leaky due to the presence of the whole grating layer. The grating with a larger modulation depth can cause a faster leaking and less interference, leading to a broader filtering response.

In our device structure, the LC PG acts as both a waveguide layer and a phase-matching medium. The LC PG layer can be approximately treated as a uniform layer with the effective refractive index denoted by n_{eff} . Thus, this periodic anisotropic waveguide can be regarded as a three-layer homogeneous waveguide. Due to the grating diffraction, each diffracted order has a corresponding tangential propagation constant determined by the grating equation. When a diffracted order is phase matched to a leaky mode in the symmetric waveguide, the grating periodicity Λ , the incident wavelength λ_0 , and the incident angle θ_{inc} are constrained by:

$$\frac{2\pi}{\lambda_0}n < \left| \frac{2\pi}{\lambda_0}n \sin \theta_{\text{inc}} - m \frac{2\pi}{\Lambda} \right| < \frac{2\pi}{\lambda_0}n_{\text{eff}}, \quad (23)$$

where n is the refractive index of the cover glass, which is set to be 1.52, and m is the diffraction order. Here, the target incident angle θ_{inc} is 0° . The geometrical parameters of the LC PG that response to red wavelengths are as follows: the grating periodicity $\Lambda = 400$ nm and thickness $d = 1.591$ μm , respectively. Three commercial LC mixtures, E44, E7 and MLC-9200-100 are selected as examples to present our novel polarization independent design. Their measured refractive indices [n_e , n_o] are [1.7806, 1.5245], [1.7378, 1.5188], and [1.6039, 1.4908] at $\lambda_0=633$ nm and 20°C , respectively [23]. To study the polarization dependence of this anisotropic structure, the polarization state of the incident light at normal incidence is expressed using Jones vector:

$$J = \begin{bmatrix} \cos \alpha \\ \sin \alpha \cdot e^{i\beta} \end{bmatrix}, \quad (24)$$

where $\tan(\alpha)$ represents the amplitude ratio of E_y to E_x , and β is the relative phase angle between E_y and E_x . For each polarization state, the corresponding reflectance can be obtained via anisotropic RCWA. For three LC mixtures, the calculated reflectance at normal incidence is all polarization independent one hundred percent, as shown in Fig. 2.

The field distribution in Fig. 3(a) shows that when the light is incident from the bottom glass substrate ($z < 0$), the electric field within the subwavelength E44 PG ($0 < z < d$) is enhanced more than 30x due to the coupling between ± 1 diffraction orders and evanescent waves. Due to normal incidence, two counterpropagating diffraction orders can be simultaneously excited, generating a standing-wave pattern along the x direction [8], as illustrated in Fig. 3(a). When the incident wavelength is 635.00 nm, which is away from the resonance wavelength of 628.71 nm, Fig. 3(b) depicts a rather weak resonant process where the electric field enhancement within the E44 PG is much less than that in Fig. 3(a). Thus, the field distribution in Fig. 3(b) can be almost equivalent to that in a single-layer uniform film sandwiched two glass substrates. In Fig. 3, the mode type is unknown because the field components are not revealed. Due to off-diagonal elements in the $[\varepsilon]$ tensor, it is not possible to split the modes into a pure TE or TM mode, and thus the modes are hybrid [24]. Figure 4 shows that right-handed circularly polarized (RCP) light and left-handed circularly polarized (LCP) light are coupled into the same HE_2 (TE_2 is dominant) hybrid mode. This polarization independent coupling to the hybrid mode gives rise to the polarization independent resonance location and bandwidth.

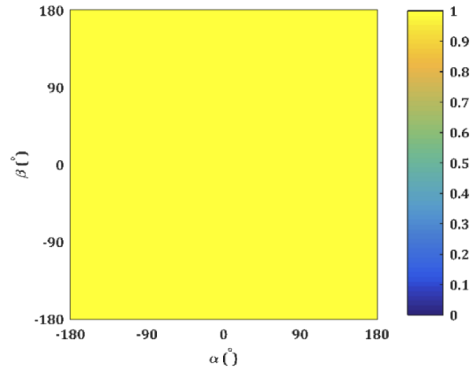


Fig. 2. The reflectance for normally incident light with all polarization states defined by J .

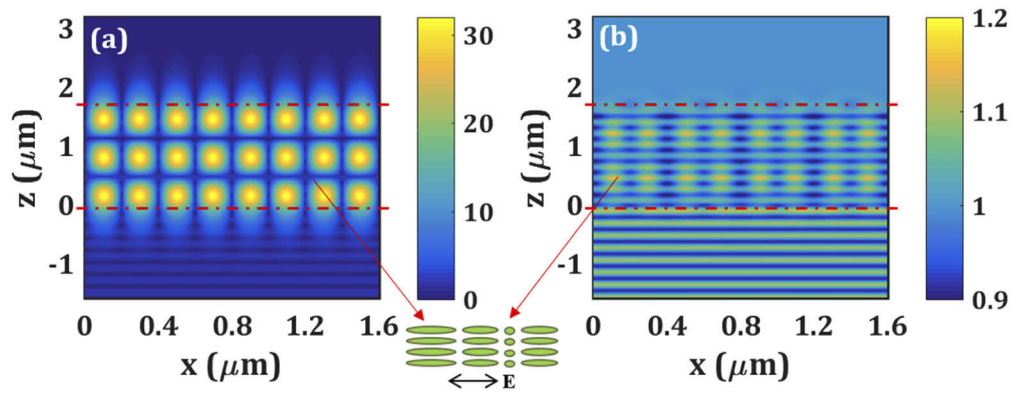


Fig. 3. The relative electric field $|E/E_0|$ generated by RCWA with light polarized along the x axis (a) at a resonance wavelength of 628.71 nm, and (b) at a wavelength of 635.00 nm.

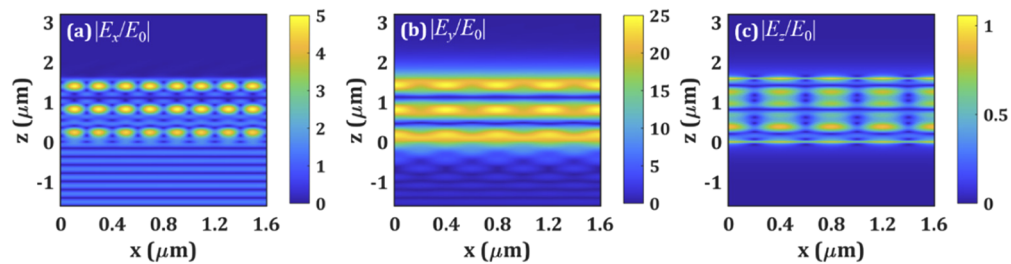


Fig. 4. The relative electric field of (a) $|E_x/E_0|$, (b) $|E_y/E_0|$, and (c) $|E_z/E_0|$ for RCP and LCP lights at a resonance wavelength of 628.71 nm.

The spectral and angular bandwidths, and the LC birefringence effect on the GMR are thoroughly examined in the following. As calculated from Fig. 5, the spectral bandwidth defined by the full width at half-maximum for the reflectance at normal incidence is 0.135 nm. Figure 5 manifests a narrow spectral and angular width, within which the reflectance is very high. Away from normal incidence, a degenerate reflectance vs. wavelength curve is split into two branches, which means there are two wavelengths corresponding to the reflectance maximum at a fixed angle. This splitting phenomenon is predicted by Eq. (23).

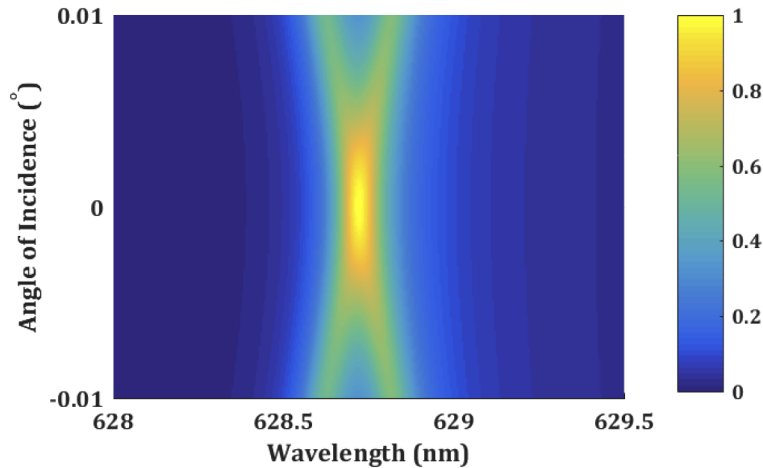


Fig. 5. Spectral and angular response of the GMR at E44 LC PG.

The wavelength dependent reflectance for E7, which has a smaller Δn than E44, is calculated to study the LC birefringence effect on the spectral bandwidth of GMR. Within the wavelength ranging from 620 nm to 650 nm, the ± 1 diffraction orders can be phase-matched to several hybrid leaky modes, as indicated in Fig. 6. Polarization independent resonance location and bandwidth is demonstrated due to the fully overlapping reflectance vs. wavelength curve for the RCP and LCP. Due to different spectral bandwidths corresponding to different modes, we select the same HE_1 mode for E7 and E44 to compare their bandwidths. As calculated from Fig. 6, their bandwidths corresponding to the HE_1 mode are 0.255 nm and 0.320 nm, respectively. This can be explained using multiple-beam interference similar to a Fabry-Perot interferometer. The larger the Δn , the higher the grating refractive index contrast. A higher index contrast increases the grating diffraction strength and thus causes a faster leaking and less interference, giving rise to a broader spectral bandwidth.

Inspired by the different spectral bandwidth, we also study how Δn affects the electric field enhancement. The same HE_1 mode is used for comparing the enhancement effect. A 30x field enhancement is obtained within the PG based on a low Δn TFT LC mixture, MLC-9200-100 at a resonant wavelength of 610.13 nm, as Fig. 7(a) shows. For the E44 PG, Fig. 7(b) manifests a 22x field enhancement at a resonant wavelength of 644.00 nm, which is smaller than that in the MLC-9200-100 PG. A lower index contrast due to a smaller Δn will decrease the leaking speed of the ± 1 diffraction order and thus induce the stronger coupling between evanescent waves and ± 1 diffraction waves.

Considering making a real device, the fabrication method is briefly described as follows [18]. Two glass substrates are first coated with a photoalignment layer (PAL) and then assembled to form a LC cell. The cell gap is controlled by spacers. To generate desired patterns, the LC cell is exposed with a linearly polarized light whose polarization direction is linearly changing over the distance. Afterwards, the LC mixture is injected into the LC cell via capillary action and the

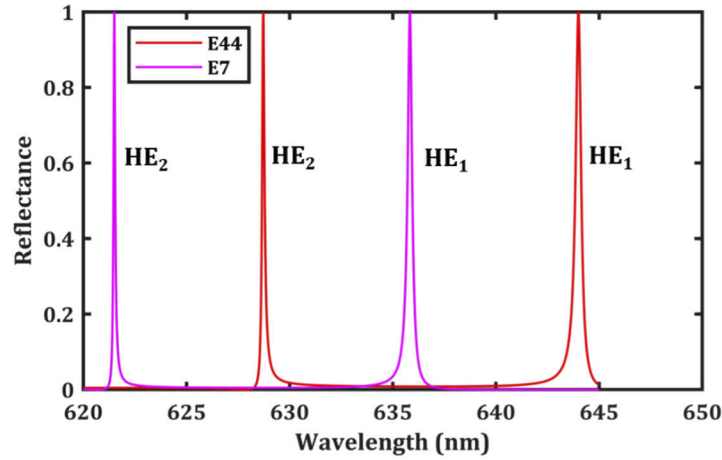


Fig. 6. Wavelength dependent reflectance for two LC mixtures, E44 and E7 with different Δn values.

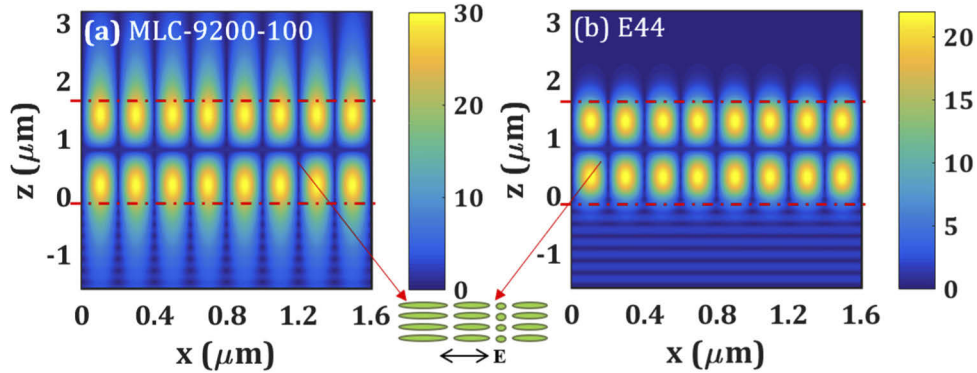


Fig. 7. The relative electric field $|E/E_0|$ generated by RCWA with light polarized along the x axis for (a) MLC-9200-100, and (b) E44.

LC directors will be orientated according to the patterned direction due to surface anchoring from the PAL. For this kind of fabrication method, the most challenging part is the alignment of the LC directors. Due to such a short periodicity, surface anchoring from the PAL may not be strong enough to align all the LC molecules well. An alternative fabrication method to provide better LC alignment is based on stacked polymer films. First, we spin-coat a PAL on a cleaned glass substrate. Next, we expose the PAL using a linearly polarized light with spatial-variant polarization directions. Then we prepare a LC reactive mesogen precursor by mixing solvent, monomer, photoinitiator, and surfactant. We spin-coat the mixture on the patterned PAL to align the LC directors. An ultra-violet light is finally used to polymerize the mixture. The same steps can be applied for depositing more polymerized layers to achieve a certain film thickness.

4. Conclusion

In conclusion, we have theoretically demonstrated the polarization independent GMR in LC based PGs. The proposed structure for realizing polarization independent GMRs is a single-layer LC PG between two glass substrates. Three commercial LC mixtures are selected as calculation examples to validate our novel method. Ultra-narrow spectral bandwidths and strong field

enhancements, along with polarization independent resonance location and bandwidth are all observed through anisotropic RCWA calculations. The LC birefringence effect on the GMR is also revealed.

Funding

Intel Corporation.

Disclosures

The authors declare no conflicts of interest.

References

1. S. S. Wang, M. G. Moharam, R. Magnusson, and J. S. Bagby, "Guided-mode resonances in planar dielectric-layer diffraction gratings," *J. Opt. Soc. Am. A* **7**(8), 1470–1474 (1990).
2. G. Quaranta, G. Basset, O. J. F. Martin, and B. Gallinet, "Recent Advances in Resonant Waveguide Gratings," *Laser Photonics Rev.* **12**(9), 1800017 (2018).
3. Z. S. Liu, S. Tibuleac, D. Shin, P. P. Young, and R. Magnusson, "High-efficiency guided-mode resonance filter," *Opt. Lett.* **23**(19), 1556–1558 (1998).
4. S. Tibuleac and R. Magnusson, "Reflection and transmission guided-mode resonance filters," *J. Opt. Soc. Am. A* **14**(7), 1617–1626 (1997).
5. L. Qian, D. Zhang, B. Dai, Q. Wang, Y. Huang, and S. Zhuang, "Optical notch filter with tunable bandwidth based on guided-mode resonant polarization-sensitive spectral feature," *Opt. Express* **23**(14), 18300–18309 (2015).
6. A. A. Mehta, R. C. Rumpf, Z. A. Roth, and E. G. Johnson, "Guided Mode Resonance Filter as a Spectrally Selective Feedback Element in a Double-Cladding Optical Fiber Laser," *IEEE Photonics Technol. Lett.* **19**(24), 2030–2032 (2007).
7. M. Paulsen, S. Jahns, and M. Gerken, "Intensity-based readout of resonant-waveguide grating biosensors: Systems and nanostructures," *Photonics and Nanostructures - Fundamentals and Applications* **26**, 69–79 (2017).
8. C. Wei, S. Liu, D. Deng, J. Shen, J. Shao, and Z. Fan, "Electric field enhancement in guided-mode resonance filters," *Opt. Lett.* **31**(9), 1223–1225 (2006).
9. A. Pokhriyal, M. Lu, V. Chaudhery, C.-S. Huang, S. Schulz, and B. T. Cunningham, "Photonic crystal enhanced fluorescence using a quartz substrate to reduce limits of detection," *Opt. Express* **18**(24), 24793–24808 (2010).
10. S. Peng and G. M. Morris, "Resonant scattering from two-dimensional gratings," *J. Opt. Soc. Am. A* **13**(5), 993–1005 (1996).
11. S. Peng and G. M. Morris, "Experimental demonstration of resonant anomalies in diffraction from two-dimensional gratings," *Opt. Lett.* **21**(8), 549–551 (1996).
12. A. Mizutani, H. Kikuta, K. Nakajima, and K. Iwata, "Nonpolarizing guided-mode resonant grating filter for oblique incidence," *J. Opt. Soc. Am. A* **18**(6), 1261–1266 (2001).
13. K. Kintaka, T. Majima, K. Hatanaka, J. Inoue, and S. Ura, "Polarization-independent guided-mode resonance filter with cross-integrated waveguide resonators," *Opt. Lett.* **37**(15), 3264–3266 (2012).
14. Y. Ding and R. Magnusson, "Resonant leaky-mode spectral-band engineering and device applications," *Opt. Express* **12**(23), 5661–5674 (2004).
15. X. Hu, K. Gong, T. Sun, and D. Wu, "Polarization-Independent Guided-Mode Resonance Filters under Oblique Incidence," *Chin. Phys. Lett.* **27**(7), 074211 (2010).
16. G. Sun and Q. Wang, "Electrically tunable polarization-independent visible transmission guided-mode resonance filter based on polymer-dispersed liquid crystals," *Microw. Opt. Technol. Lett.* **62**(12), 3727–3732 (2020).
17. D. C. Zografopoulos, E. E. Kriezis, and R. Beccherelli, "Design of Switchable Guided-Mode Resonant Filters in Zenithal-Bistable Liquid-Crystal Gratings," *IEEE Photonics Technol. Lett.* **29**(16), 1367–1370 (2017).
18. T. Zhan, Y.-H. Lee, G. Tan, J. Xiong, K. Yin, F. Gou, J. Zou, N. Zhang, D. Zhao, J. Yang, S. Liu, and S.-T. Wu, "Pancharatnam–Berry optical elements for head-up and near-eye displays [Invited]," *J. Opt. Soc. Am. B* **36**(5), D52–D65 (2019).
19. R. C. Rumpf, "Improved formulation of scattering matrices for semi-analytical methods that is consistent with convention," *Prog. Electromagn. Res. B* **35**, 241–261 (2011).
20. M. G. Moharam and T. K. Gaylord, "Rigorous coupled-wave analysis of planar-grating diffraction," *J. Opt. Soc. Am. A* **71**(7), 811–818 (1981).
21. S. Tibuleac and R. Magnusson, "Narrow-linewidth bandpass filters with diffractive thin-film layers," *Opt. Lett.* **26**(9), 584–586 (2001).
22. Y. Huang, T. X. Wu, and S. T. Wu, "Simulations of liquid-crystal Fabry-Perot etalons by an improved 4×4 matrix method," *J. Appl. Phys.* **93**(5), 2490–2495 (2003).
23. J. Li, C.-H. Wen, S. Gauza, R. Lu, and S.-T. Wu, "Refractive Indices of Liquid Crystals for Display Applications," *J. Disp. Technol.* **1**(1), 51–61 (2005).
24. J. Beckckman, R. James, F. A. Fernandez, W. De Cort, P. J. M. Vanbrabant, and K. Neyts, "Calculation of Fully Anisotropic Liquid Crystal Waveguide Modes," *J. Lightwave Technol.* **27**(17), 3812–3819 (2009).